

Boltzmann approach to collective motion via nonlocal visual interaction

Susumu Ito and Nariya Uchida*

Department of Physics, Tohoku University, Sendai, 980-8578, Japan

(Dated: March 18, 2025)

Visual cues play crucial roles in the collective motion of animals, birds, fish, and insects. The interaction mediated by visual information is essentially non-local and has many-body nature due to occlusion, which poses a challenging problem in modeling the emergent collective behavior. In this paper, we introduce a Boltzmann-equation approach incorporating non-local visual interaction. Occlusion is treated in a self-consistent manner via a coarse-grained density field, which renders the interaction effectively pairwise. Our model also incorporates the recent finding that each organism stochastically selects a neighbor to interact at each instant. We analytically derive the order-disorder transition point, and show that the visual screening effect raises the transition threshold, which does not vanish when the density of the agents or the range of the intrinsic interaction is taken to infinity. Our analysis suggests that the model exhibits a discontinuous transition as in the local interaction models, and but the discontinuity is weakened by the non-locality. Our study clarifies the essential role of non-locality in the visual interactions among moving organisms.

I. INTRODUCTION

Collective motion is ubiquitously found in Nature [1]. Visual information plays an important role in the interaction between organisms that have eyes: insects [2], fish [2, 3], birds [4], and humans [5]. In the visual interaction, each organism often selects a specific neighbor to interact with and decides its next motion [2, 5, 6]. The selective decision-making reduces the load on the information processing system in the brain [7]. A recent study proposes a mechanism of stochastic pairwise interaction, in which each individual randomly selects another and copy its orientation [8].

Agent-based models are a powerful tool to simulate collective motion [9–11]. Some of them consider visual information under the assumption that each agent interacts with all detected neighbors simultaneously [4, 12–15]. Several other models incorporate selective decision-making, and reproduce experimental results for specific organisms [2, 5, 16–18].

Continuum description has also been used to elucidate the nature of phase transitions in conventional models of collective motion [19–24]. In particular, the Boltzmann approach, which describes time evolution of a probability distribution function by pairwise collision and alignment of agents, is successfully used to derive hydrodynamic equations and analyze phase transition [21–24]. However, fundamental aspects of phase transition arising from visual interaction is not yet clear. The difficulty lies in the many-body nature of occlusion, where the interaction between two individuals is screened by the other individuals in between.

In this paper, we introduce a Boltzmann approach to collective motion induced by non-local visual interaction. Motivated by the experimental finding [8], we assume that an agent randomly selects a distant neighbor and

one at a time, which has good affinity with the framework of the Boltzmann equation. We incorporate occlusion by coarse-graining the clouds of intervening agents as a density field, which is self-consistently determined by the Boltzmann equation. This results in an effective pairwise interaction between agents. In the absence of occlusion, the probability to select a neighbor decays with a characteristic distance determined by the resolution of the eye system. We analytically derive the order-disorder transition point, and show that it is shifted by the visual screening effect. Furthermore, we find that the non-locality of interaction suppresses the discontinuity of the phase transition in comparison to local collision models [21, 25], and that the polar order parameter exhibits a mean-field critical behavior in the weak-advection limit and in a finite system.

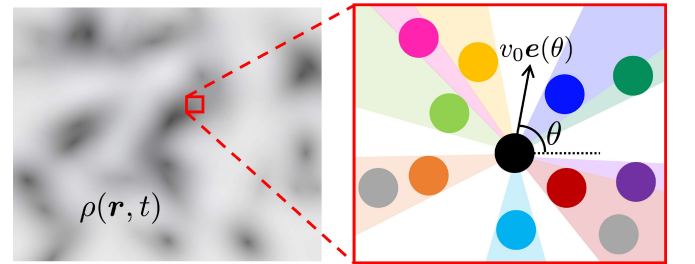


FIG. 1. Schematic illustration of the model. The left panel shows the clouds of agents described by the density field $\rho(\mathbf{r}, t)$ in the continuum description, and the right panel shows the discrete picture. Each agent has a circular shape and moving with the velocity $v_0 \mathbf{e}(\theta)$. The center agent (black) perceives the neighbors and interacts with one of them at a time. The agents shown in gray are not seen by the black agent due to occlusion.

* uchida@cmpt.phys.tohoku.ac.jp

II. MODEL

A. Boltzmann equation

We consider a two-dimensional model where each agent is described by its position $\mathbf{r} = (x, y)$ and direction of motion $\mathbf{e}(\theta) = (\cos \theta, \sin \theta)$. For simplicity, we assume that each agent moves with a constant speed v_0 and its shape is a circle of diameter D (see Fig. 1). We define the probability distribution function $f(\mathbf{r}, \theta, t)$ and the number density of agents $\rho(\mathbf{r}, t) = \int_{-\pi}^{\pi} d\theta f(\mathbf{r}, \theta, t)$.

The Boltzmann equation describes time evolution of f via the self-diffusion term $I_{\text{self}}[f]$ and visual interaction term $I_{\text{vis}}[f]$ as follows:

$$\frac{\partial f}{\partial t} + v_0 \mathbf{e}(\theta) \cdot \nabla f = I_{\text{self}}[f] + I_{\text{vis}}[f], \quad (1)$$

$$I_{\text{self}}[f] = -s f(\mathbf{r}, \theta, t) + s \int_{-\pi}^{\pi} d\theta' p(\theta - \theta') f(\mathbf{r}, \theta', t), \quad (2)$$

$$I_{\text{vis}}[f] = -c \int d^2 \mathbf{r}' \int_{-\pi}^{\pi} d\theta' G(\mathbf{r}, \mathbf{r}' - \mathbf{r}, t) \Gamma(|\mathbf{r}' - \mathbf{r}|, \theta' - \theta) f(\mathbf{r}, \theta, t) f(\mathbf{r}', \theta', t) \\ + c \int d^2 \mathbf{r}' \int_{-\pi}^{\pi} d\theta_1 \int_{-\pi}^{\pi} d\theta_2 G(\mathbf{r}, \mathbf{r}' - \mathbf{r}, t) \Gamma(|\mathbf{r}' - \mathbf{r}|, \theta_2 - \theta_1) f(\mathbf{r}, \theta_1, t) f(\mathbf{r}', \theta_2, t) \hat{p}(\theta - \vartheta(\theta_1, \theta_2)). \quad (3)$$

In the self-diffusion integral (Eq. (2)), s is the rate of reorientation by the noise, and $p(\theta)$ is the probability distribution function of angle change: we use the von Mises distribution $p(\theta) = e^{\kappa \cos \theta} / (2\pi I_0(\kappa))$, where $I_{n=0,1,\dots}(\kappa)$ is the modified Bessel function of the first kind and κ is the sharpness parameter [16]. In Eq. (2), the first and second term on the right-hand side represents the probability of transition from θ to any angle and from θ' to θ , respectively.

The visual interaction integral (Eq. (3)) describes the pairwise orientational interaction between the agent at \mathbf{r} and a neighbor at \mathbf{r}' . The rate of interaction is determined by occlusion by other agents and the intrinsic mechanism of visual recognition. The latter decays with distance due to the resolution of eyes [26] and also depends on the relative direction of motion [27]. Therefore, we introduce the occlusion factor $G(\mathbf{r}, \mathbf{R}, t)$ and the intrinsic factor $\Gamma(|\mathbf{R}|, \psi)$ in the interaction kernel, where $\mathbf{R} = \mathbf{r}' - \mathbf{r}$ and $\psi = \theta' - \theta$ ($\psi = \theta_2 - \theta_1$) are the relative position and angle, respectively. We will formulate them in the following paragraphs. In Eq. (3), c is the reference interaction rate, and $\hat{p}(\theta) = e^{\hat{\kappa} \cos \theta} / (2\pi I_0(\hat{\kappa}))$ is the probability distribution function of angle change for interaction [28]. The first term on the right-hand side represents the outgoing event in which the agent at (\mathbf{r}, θ) interacts with the neighbor at (\mathbf{r}', θ') and is reoriented from θ to another angle. The second term represents the incoming event where the agent at (\mathbf{r}, θ_1) interacts with the neighbor at (\mathbf{r}', θ_2) and is reoriented to their average angle $\theta = \vartheta(\theta_1, \theta_2) = \arg(e^{i\theta_1} + e^{i\theta_2})$ [21].

B. occlusion factor

Now we formulate the occlusion factor $G(\mathbf{r}, \mathbf{R}, t)$, which is a key feature of our model. The resolution of the eye is limited by the number of ganglion cells in the

retina [26], and represented by the azimuthal resolution angle Φ in our two-dimensional model. Images of the other agents within the angle Φ centered around the line of sight, which has the direction $\hat{\mathbf{R}} = \mathbf{R}/R$, are not distinguished from each other. We define the angular width $\Phi_G(\mathbf{r}, \mathbf{R}, t)$ of the regions that are *not* occupied by the images of the other agents within the distance R and within the angle Φ (see Fig. 2). The occlusion factor $G(\mathbf{r}, \mathbf{R}, t)$ is defined as the probability that a neighbor at

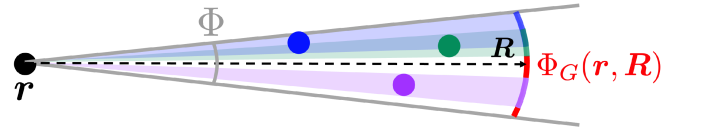


FIG. 2. Schematic illustration of $\Phi_G(\mathbf{r}, \mathbf{R})$. The agent at the position \mathbf{r} sees the point at the relative position \mathbf{R} on the line of sight. The images of the neighbors (the blue, green, and purple agents) in the angle Φ are projected onto the arc, in which the non-occupied parts (red) has the total angle $\Phi_G(\mathbf{r}, \mathbf{R})$.

$\mathbf{r} + \mathbf{R}$ is visible for the agent at \mathbf{r} . Therefore, it reads

$$G(\mathbf{r}, \mathbf{R}, t) = \frac{\Phi_G(\mathbf{r}, \mathbf{R}, t)}{\Phi} \leq 1. \quad (4)$$

As the distance is increased in a given direction $\hat{\mathbf{R}}$, more agents come into the line of sight and decrease $\Phi_G(\mathbf{r}, \mathbf{R}, t)$. Let $\sigma(\mathbf{r}, \mathbf{R}, t)dR$ be the fraction of the angular region occupied by the agents in the distance between R and $R + dR$ and within the angle Φ . Given that they are randomly distributed, the unoccupied angular region Φ_G is reduced by the same fraction. Thus we obtain the differential equation

$$\frac{\partial}{\partial R} \Phi_G(\mathbf{r}, \mathbf{R}, t) = -\sigma(\mathbf{r}, \mathbf{R}, t) \Phi_G(\mathbf{r}, \mathbf{R}, t). \quad (5)$$

The occupied fraction is related to the local density as

$$\sigma(\mathbf{r}, \mathbf{R}, t) = \mathcal{D}(R) \rho(\mathbf{r} + \mathbf{R}, t), \quad (6)$$

where $\mathcal{D}(R)$ is the average arc length occupied by an agent in the visual angular bin Φ . This fraction is calculated as the angle occupied by a single agent \mathcal{D}/R multiplied by the number of agents in the area $\rho R \Phi dR$ and divided by the angular width Φ . While the angle occupied by a single agent in the field of view of a focal agent tends to zero in the limit $R \rightarrow \infty$, the average length of the occupied visual arc length \mathcal{D} goes to the diameter of the agent D . At short distances, an agent covers the whole angular width Φ and thus \mathcal{D} is given by the arc length $R\Phi$. The formula for intermediate distances is derived by straightforward geometric calculation [29], and gives

$$\mathcal{D}(R) = \begin{cases} R\Phi & [R < R_D], \\ R_D\Phi \left(2 - \frac{R_D}{R}\right) & [R > R_D], \end{cases} \quad (7)$$

where $R_D = D/(2\Phi)$.

The differential equation (5) is solved under the boundary condition $\Phi_G|_{R \rightarrow 0} = \Phi$. Substituting the solution into Eq.(4), we obtain

$$G(\mathbf{r}, \mathbf{R}, t) = \exp\left(-\int_0^R dR' \mathcal{D}(R') \rho(\mathbf{r} + \mathbf{R}', t)\right), \quad (8)$$

The occlusion factor (Eq. (8)) gives an effective pairwise interaction mediated by the density field ρ , which is determined by the Boltzmann equation in a self-consistent manner.

Note that the coarse-grained description requires that many neighbors are observed in the resolution angle Φ . For the mean density ρ_0 , a neighbor in the typical distance $R \sim 1/\sqrt{\rho_0\Phi}$ (note that the number of agents in the distance R and angle Φ is estimated by $n \sim \rho_0 R^2 \Phi/2$) occupies the angle $\sqrt{\rho_0\Phi}D$ in the field of view, which should be much smaller than Φ . Thus we obtain the condition $\rho_0 \ll \Phi/D^2$ for the density. Under this condition, $R \gg R_D$ is satisfied in Eq. (7) for most cases,

and the occlusion factor G decays with the characteristic distance $R_{\text{occ}} = 1/(\rho_0 D) \gg R$ [30]. Since $\Phi \ll 1$, the above condition also ensures that the area fraction $A = \rho_0 \pi (D/2)^2$ is much smaller than unity, which is required for the excluded-volume interaction to be negligible.

C. intrinsic factor

The intrinsic factor $\Gamma(R, \psi)$ depends on the relative distance R and the relative angle ψ . We assume that it can be factorized as $\Gamma(R, \psi) = B(R)K(\psi)$. The factor $B(R)$ represents the possibility of visual recognition of the direction of motion of a neighbor. The probability of visual recognition decreases as the relative distance increases. We then define

$$B(R) = \exp\left(-\frac{R^2}{2R_0^2}\right), \quad (9)$$

and R_0 is the characteristic distance of the visual recognition. In fact, the magnitude of orientational interaction of some species of fish is found to obey the Gaussian function [27].

The factor $K(\psi)$ represents the probability of reaction to a neighbor at the relative angle ψ . The detailed study for fish [27] shows

$$K(\psi) = \frac{|\sin \psi| \{1 + a \cos(2\psi)\}}{\sqrt{(2 - 2a + a^2)/4}}, \quad (10)$$

where the essential term is $|\sin \psi|$ and the $\cos(2\psi)$ term is introduced for fitting with the experimental data [27]. The normalization $\frac{1}{2\pi} \int_{-\pi}^{\pi} d\psi K^2(\psi) = 1$ is assumed. In this paper, we use

$$K(\psi) = \sqrt{2} |\sin \psi| \quad (11)$$

by setting $a = 0$ for simplicity and in order to make our model more applicable to various organisms [31].

III. RESULTS

A. linear stability

As we increase the interaction rate c , the uniform disordered state $f = \bar{f}_0$ (const.) becomes unstable. In order to obtain the transition point $c = c_{\text{tr}}$, we performed a linear stability analysis of the Boltzmann equation (see Appendix 5). We add the perturbation $\delta f(\mathbf{r}, \theta, t)$ to ρ_0 , and define its Fourier component $\delta f_k(\mathbf{q})$ and the complex damping rate $\Lambda_k(\mathbf{q})$ via:

$$\delta f(\mathbf{r}, \theta, t) = \int d^2 \mathbf{q} \sum_k \delta f_k(\mathbf{q}) e^{i(\mathbf{q} \cdot \mathbf{r} + k\theta)} e^{-\Lambda_k(\mathbf{q})t}, \quad (12)$$

where $k = 0, \pm 1, \pm 2, \dots$ is the index of the Fourier modes in the angular domain. From the stability analysis, we

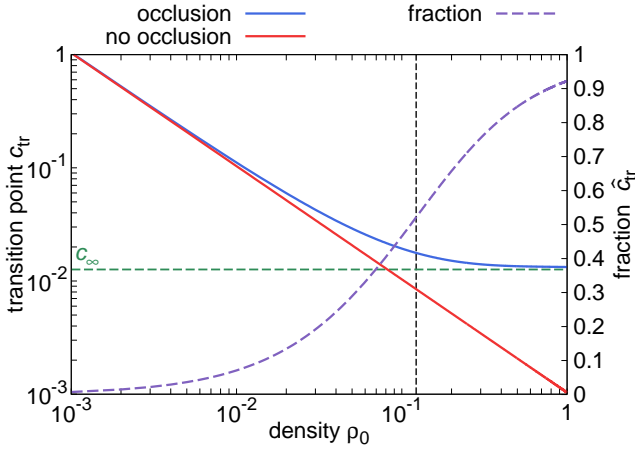


FIG. 3. The transition point c_{tr} as a function of the density ρ_0 . We set the biologically reasonable parameter values $s = 2$, $\kappa = 6$, $\hat{\kappa} = 20$, $\Phi = 7^\circ$, $R_0 = 10$ [16, 26, 27, 32, 33] which are rescaled by the diameter $D = 1$ body length and 1 sec [34]. The blue solid line shows c_{tr} (Eq. (15)), and reaches the horizontal green dashed line c_∞ in high density limit. Note that the theory is valid only for $\rho_0 \ll \Phi/D^2$, and the black dashed line marks $\rho_0 = \Phi/D^2 \simeq 0.12$. The red solid line corresponds to the no occlusion case $c_{\text{tr}}|_{D=0}$. The purple dashed line is the fraction \hat{c}_{tr} to the right vertical axis.

find that only the damping rate of the mode $k = \pm 1$ can become negative. Their damping rate is given by

$$\text{Re } \Lambda_{\pm 1}(\mathbf{q}) = s(1 - 2\pi p_1) - 4\sqrt{2}c\mathcal{I}\bar{f}_0 \left\{ \frac{2}{3}(2\pi\hat{p}_1) \left(1 + \hat{\mathcal{I}}(\mathbf{q}) \right) - 1 \right\}, \quad (13)$$

where p_1 and \hat{p}_1 are the Fourier components of $p(\theta)$ and $\hat{p}(\theta)$ for $k = 1$, respectively, and

$$\mathcal{I}\bar{f}_0 = \frac{1 - \exp\left(-\frac{\rho_0 R_D^2}{2} \left(\Phi + \frac{1}{\rho_0 R_0^2} \right)\right)}{\Phi + \frac{1}{\rho_0 R_0^2}} + \rho_0 R_D^2 \int_1^\infty d\xi \xi e^{-\frac{R_D^2}{2R_0^2} \xi^2} \left(e^{\frac{3}{2}\xi} e^{-2\xi} \right)^{\rho_0 \Phi R_D^2}. \quad (14)$$

is a function of the dimensionless quantities $\rho_0 R_D^2$, $\rho_0 R_0^2$, and Φ . In Eq. (13), the wavenumber-dependent function $\hat{\mathcal{I}}(\mathbf{q})$ satisfies $-1 < \hat{\mathcal{I}}(\mathbf{q}) \leq 1$, and has the single maximum $\hat{\mathcal{I}}(\mathbf{0}) = 1$. Thus the transition point is determined by $\text{Re } \Lambda_1(\mathbf{0}) = 0$. In the no-occlusion case obtained in the point particle limit $D = 0$, we get $\hat{\mathcal{I}}(\mathbf{q}) = e^{-q^2 R_0^2/2}$. In the linear stability analysis, we neglected the advection term in Eq.(1), which does not affect the transition point [21, 24] (see also Appendix 5).

B. transition point

We then obtain the transition point

$$c_{\text{tr}} = \frac{s}{4\sqrt{2}\mathcal{I}\bar{f}_0} \frac{1 - 2\pi p_1}{\frac{4}{3}(2\pi\hat{p}_1) - 1} := \frac{c_0}{\mathcal{I}\bar{f}_0}, \quad (15)$$

where c_0 increases when s increases, or when κ or $\hat{\kappa}$ decreases, which means that the transition is hindered by the orientational noise. Note that $2\pi\hat{p}_1$ must be larger than $3/4$ such that $c_0 > 0$. As shown in Fig. 3, c_{tr} decreases as ρ_0 increases, which meets the expectation that a higher density of agents induces stronger alignment. It is notable that c_{tr} is non-zero in the limit $R_0 \rightarrow \infty$, where the interaction decays only due to occlusion. In contrast, for $D = 0$, we obtain $c_{\text{tr}}|_{D=0} = c_0/(\rho_0 R_0^2)$, which vanishes in the limit $R_0 \rightarrow \infty$.

In Fig. 3, we also show the fraction $\hat{c}_{\text{tr}} = (c_{\text{tr}} - c_{\text{tr}}|_{D=0})/c_{\text{tr}}$. As a function of the density, it shows a sizable increase before reaching the limit of validity of the model $\rho_0 = \Phi/D^2$, and then converges to unity as $\rho_0 \rightarrow \infty$.

IV. DISCUSSIONS

We summarize the new aspects of our analytical treatment in comparison with previous Boltzmann-type models of active matter as follows: (i) We have modeled the visual interaction by the Boltzmann approach for the first time. (ii) The screening effect (occlusion) is represented by a density field, which is self-consistently determined from the distribution function. This has enabled the effective description of many-body interaction in the Boltzmann approach. Except for occlusion, the interaction is assumed to be pairwise, which is justified by the experimental observation in Ref. [8]. We incorporated the non-local visual interaction to the Boltzmann equation as the effective pairwise interaction. Our model shows that the visual screening effect raises the transition threshold for the interaction rate c , which becomes non-zero even in the limits of high density or infinite range of the intrinsic interaction. This result is in stark contrast to those of the local-interaction models that assume point-like particles [21, 23]. In those models, the transition threshold was determined by hydrodynamic equations that are obtained by truncating the hierarchical equations for the angular Fourier modes $f_k(\mathbf{r}, t) = (2\pi)^{-1} \int_{-\pi}^{\pi} f(\mathbf{r}, \theta, t) e^{-ik\theta} d\theta$. Our results reproduce those of the previous models of polar particles with ferromagnetic interactions by taking the local limit $R_0 \rightarrow 0$ with cR_0^2 kept constant. In this limit, the interaction kernel $I_{\text{vis}}[f]$ converges to the delta function $\delta(\mathbf{r}' - \mathbf{r})$ [36], and the linear growth rate $-\text{Re } \Lambda_1(\mathbf{0})$ becomes identical to μ of Eq. (31) in Ref. [21].

The damping rate $\text{Re } \Lambda_1$ also contains the information of the kind of the disorder-order phase transition. In previous local interaction models, instability of the

modes with $\mathbf{q} \neq \mathbf{0}$ induce phase coexistence in the form of traveling bands, which is the origin of the discontinuous transition [21]. Therefore, the transition is continuous if the $\mathbf{q} \neq \mathbf{0}$ modes are linearly stable at the transition point. This holds if the damping rate has no density-dependence, which is the case for metric-free interactions [22]. On the other hand, the transition becomes discontinuous if the damping rate depends on the density [22]. In our model, we have $\partial\Lambda_1/\partial\rho_0 \neq 0$ and thus our system shows a discontinuous transition. The non-locality of the interaction does not affect the kind of the phase transition. This is reasonable if we consider that the Vicsek model [9] has a finite interaction range and shows a discontinuous transition [11]. Active nematics with non-local repulsion also shows a discontinuous order-disorder transition [24]. It is also worth mentioning that the visual interaction with occlusion in high density regions resembles metric-free interactions with the nearest topological neighbors, which may render the transition density independent. However, recent works [37, 38] found emergence of traveling bands even for purely topological interactions, and proposed different mechanisms that induce effective density-order couplings. It suggests the possibility that the order-disorder transition in aligning active matter systems may be always discontinuous due to implicit density dependence.

Let us now consider the model's behavior above the transition point. The advection term in the Boltzmann equation (1) introduces couplings between f_k and $f_{k\pm 1}$ in the mode expansion, which introduces an infinite-dimensional matrix in the linear stability analysis. However, in our model, only the mode with $k = \pm 1$ is linearly unstable at the transition point in the non-advection limit ($v_0 = 0$). It means that there is a finite window of c above the transition point where the damping rate for $f_{k \neq \pm 1}$ remains positive. In this window, contributions to $f_{|k|>1}$ by the advective couplings are $\mathcal{O}(v_0^{|k|-1} f_{\pm 1})$, which we can neglect compared to non-advection terms for sufficiently small values of v_0 . Thus we can use the damping rate $\Lambda_k(\mathbf{q})$ obtained in the non-advection limit ($v_0 = 0$).

In our model, the wavenumber-dependence of the damping rates comes through $\hat{I}(\mathbf{q})$ in Eq. (13). Since $\hat{I}(\mathbf{q})$ is a decreasing function of q and R_0 , only long-wavelength modes are destabilized in the vicinity of the transition point, and the unstable range of q gets narrower for a larger interaction range. In particular, when we consider a finite two-dimensional system with the periodic boundary condition, the wavenumber is discretized and there is a finite window of c above c_{tr} where only the $\mathbf{q} = \mathbf{0}$ mode becomes unstable. In this case, the transition becomes continuous and we can calculate the polar order parameter defined by $P = \left| \int_{-\pi}^{\pi} d\theta e(\theta) \langle f(\mathbf{r}, \theta, t) \rangle \right| / \rho_0 = |\langle f_1 \rangle| / f_0$, where the

brackets mean spatiotemporal and ensemble averages. By truncating the hierarchical equations for f_k , we obtain the scaling law $P = P_0(c_{\text{tr}})(c - c_{\text{tr}})^{1/2}$ [35]. As shown in Fig. S3, the prefactor $P_0(c_{\text{tr}})$ is larger for smaller c_{tr} , which corresponds to large ρ_0 and/or large $\hat{\kappa}$.

Finally, we compare our result with the behavior of real organisms, using the examples of fish in a shallow tank showing two-dimensional collective motion. A phase transition is observed for tilapia (*O. niloticus* L.) when the number density increases above a threshold [39], which is in the range $\rho_0 \in [0.01, 0.1]$ in our model. (In Ref. [39], the number density at the transition point is 472 fishes/m² and the body length of specimens is 11-15 mm. Using the body length as the unit of length, we obtain the dimensionless density $\rho_0 = 0.057 - 0.106$ fishes/BL². Considering the slenderness of the body of real fish, which reduces occupancy in the visual field compared to the circular fish in our model, we estimate the effective density to be in the range $\rho_0 \in [0.01, 0.1]$.) For $\rho_0 = 0.01$, the fraction \hat{c}_{tr} is about 0.1, and thus occlusion has small but non-negligible effect. However, the experimental density is closer to the threshold $\rho_0 = \Phi/D^2 \simeq 0.12$, and our results are not directly applicable to the experiment. For near and above the threshold density where a few agents occupy the visual field, we can consider a hybrid model: we treat the agents as discrete self-propelled particles in the near field, and use continuum description with the probability distribution function at the far field. This will reduce the computational cost for treating many fish in the far field, and to be addressed in future work. A quantitative study of occlusion in different species of fish (or robot fish) will be necessary to verify the results of our model. On the other hand, as the number density increases, golden shiner (*N. crysoleucas*) shows rotating state [40], and cichlid (*E. suratensis*) exhibits many oriented sub-clusters which is not aligned as a whole cluster [8]. There are many aspects of interactions that are considered in previous agent-based models but not in our model. The emergence of a rotating state is facilitated by introducing the dead angle [41] and the wall [42], and considering three-dimensional motion [43]. The polar order is also disturbed by anisotropic attraction and repulsion [44], the change of speed by interaction [14, 18], and non-circular shapes of an agent [4]. The effects of these interesting extensions by modifying the spatial integral kernel in the Boltzmann equation are the subject of future work.

ACKNOWLEDGMENTS

We acknowledge financial support by JSPS KAKENHI Grant No. 23KJ0171 to S.I. and support by a research environment of Tohoku University, Division for Interdisciplinary Advanced Research and Education to S.I.

Appendix: Stability analysis of the Boltzmann equation

1. Fourier components of the distribution function

Here, we perform the linear stability analysis for Eq. (1). The aim is the derivation of the transition point. We consider the perturbation from the uniform distribution $\overline{f_0}$:

$$f(\mathbf{r}, \theta, t) = \overline{f_0} + \delta f(\mathbf{r}, \theta, t). \quad (\text{A.1})$$

The density is

$$\rho(\mathbf{r}, t) = 2\pi\overline{f_0} + \int_{-\pi}^{\pi} d\theta \delta f(\mathbf{r}, \theta, t) = \rho_0 + \delta\rho(\mathbf{r}, t), \quad (\text{A.2})$$

and the occlusion factor reads

$$G(\mathbf{r}, \mathbf{R}, t) \simeq \exp\left(-\rho_0 \int_0^R dR' \mathcal{D}(R')\right) \times \left(1 - \int_0^R dR' \mathcal{D}(R') \delta\rho(\mathbf{r} + \mathbf{R}', t)\right) := G_0(R) \{1 - \delta G(\mathbf{r}, \mathbf{R}, t)\}. \quad (\text{A.3})$$

The Boltzmann equation (Eq. (1)) becomes

$$\begin{aligned} \frac{\partial \delta f(\mathbf{r}, \theta, t)}{\partial t} = & -v_0 \mathbf{e}(\theta) \cdot \nabla \delta f(\mathbf{r}, \theta, t) \\ & -s \delta f(\mathbf{r}, \theta, t) + s \int_{-\pi}^{\pi} d\theta' p(\theta - \theta') \delta f(\mathbf{r}, \theta', t) \\ & -c\mathcal{I}\overline{f_0} \int_{-\pi}^{\pi} d\theta' K(\theta' - \theta) \\ & \times \left\{ \overline{f_0} \left(1 - \frac{\delta\mathcal{I}(\mathbf{r}, t)}{\mathcal{I}}\right) + \delta f(\mathbf{r}, \theta, t) + \frac{1}{\mathcal{I}} \int d^2\mathbf{r}' G_0(|\mathbf{r}' - \mathbf{r}|) B(|\mathbf{r}' - \mathbf{r}|) \delta f(\mathbf{r}', \theta', t) \right\} \\ & + c\mathcal{I}\overline{f_0} \int_{-\pi}^{\pi} d\theta_1 \int_{-\pi}^{\pi} d\theta_2 K(\theta_2 - \theta_1) \hat{p}(\theta - \vartheta(\theta_1, \theta_2)) \\ & \times \left\{ \overline{f_0} \left(1 - \frac{\delta\mathcal{I}(\mathbf{r}, t)}{\mathcal{I}}\right) + \delta f(\mathbf{r}, \theta_2, t) + \frac{1}{\mathcal{I}} \int d^2\mathbf{r}' G_0(|\mathbf{r}' - \mathbf{r}|) B(|\mathbf{r}' - \mathbf{r}|) \delta f(\mathbf{r}', \theta_2, t) \right\}. \end{aligned} \quad (\text{A.4})$$

where we use $K(-\psi) = K(\psi)$ and $\vartheta(\theta_1, \theta_2) = \vartheta(\theta_2, \theta_1)$ and define

$$\mathcal{I} = \int d^2\mathbf{R} G_0(R) B(R), \quad \delta\mathcal{I}(\mathbf{r}, t) = \int d^2\mathbf{R} G_0(R) B(R) \delta G(\mathbf{r}, \mathbf{R}, t). \quad (\text{A.5})$$

We define the Fourier transform for a function $F(\mathbf{r}, \theta)$:

$$F(\mathbf{r}, \theta) = \int d^2\mathbf{q} \sum_k F_k(\mathbf{q}) e^{i(\mathbf{q} \cdot \mathbf{r} + k\theta)}, \quad F_k(\mathbf{q}) = \frac{1}{(2\pi)^3} \int d^2\mathbf{r} \int_{-\pi}^{\pi} d\theta F(\mathbf{r}, \theta) e^{-i(\mathbf{q} \cdot \mathbf{r} + k\theta)}, \quad (\text{A.6})$$

where $k = 0, \pm 1, \pm 2, \dots$ is the discrete wavenumber of the angle Fourier transform, and \mathbf{q} is the wavenumber vector of the spatial Fourier transform. We introduce the damping rate $\Lambda_k(\mathbf{q})$ for the Fourier component via

$$\delta f(\mathbf{r}, \theta, t) = \int d^2\mathbf{q} \sum_k \delta f_k(\mathbf{q}) e^{i(\mathbf{q} \cdot \mathbf{r} + k\theta)} e^{-\Lambda_k(\mathbf{q})t} := \int d^2\mathbf{q} \sum_k \delta f_k(\mathbf{q}, t) e^{i(\mathbf{q} \cdot \mathbf{r} + k\theta)}. \quad (\text{A.7})$$

(The index of zero represents $k = 0$, except for $\overline{f_0}$, ρ_0 , and the parameters).

2. Terms not including δf

We confirm that the terms which do not include explicitly δf are canceled out. In other words,

$$-c\mathcal{I}\overline{f_0}^2 \left(1 - \frac{\delta\mathcal{I}(\mathbf{r}, t)}{\mathcal{I}}\right) \int_{-\pi}^{\pi} d\theta' K(\theta' - \theta) = -2\pi c\mathcal{I}\overline{f_0}^2 \left(1 - \frac{\delta\mathcal{I}(\mathbf{r}, t)}{\mathcal{I}}\right) K_0 \quad (\text{A.8})$$

and

$$c\mathcal{I}\bar{f}_0^2 \left(1 - \frac{\delta\mathcal{I}(\mathbf{r}, t)}{\mathcal{I}}\right) \int_{-\pi}^{\pi} d\theta_1 \int_{-\pi}^{\pi} d\theta_2 K(\theta_2 - \theta_1) \hat{p}(\theta - \vartheta(\theta_1, \theta_2)) \quad (\text{A.9})$$

are canceled out as follows.

The angle $\vartheta(\theta_1, \theta_2)$ is $\arg(e^{i\theta_1} + e^{i\theta_2})$ in the Boltzmann equation, but we must consider the absolute value of $e^{i\theta_1} + e^{i\theta_2}$ for accurate treatment of $\arg(\circ)$ in the Fourier transform for the calculation of $\int_{-\pi}^{\pi} d\theta_1 \int_{-\pi}^{\pi} d\theta_2 K(\theta_2 - \theta_1) \hat{p}(\theta - \vartheta(\theta_1, \theta_2))$. We therefore redefine

$$\vartheta(\theta_1, \theta_2) = \arg \left(\frac{e^{i\theta_1} + e^{i\theta_2}}{|2 \cos(\frac{\theta_2 - \theta_1}{2})|} \right), \quad (\text{A.10})$$

and the integral is

$$\begin{aligned} & \int_{-\pi}^{\pi} d\theta_1 \int_{-\pi}^{\pi} d\theta_2 K(\theta_2 - \theta_1) \hat{p}(\theta - \vartheta(\theta_1, \theta_2)) \\ &= \int_{-\pi}^{\pi} d\theta_1 \int_{-\pi}^{\pi} d\theta_2 \sum_k K_k e^{ik(\theta_2 - \theta_1)} \sum_{k'} \hat{p}_{k'} e^{ik'(\theta - \vartheta(\theta_1, \theta_2))} \\ &= \int_{-\pi}^{\pi} d\theta_1 \int_{-\pi}^{\pi} d\theta_2 \sum_k K_k e^{ik(\theta_2 - \theta_1)} \sum_{k'} \hat{p}_{k'} e^{ik'\theta} \left(\frac{e^{i\theta_1} + e^{i\theta_2}}{|2 \cos(\frac{\theta_2 - \theta_1}{2})|} \right)^{-k'} \\ &= \int_{-\pi}^{\pi} d\theta_1 \int_{-\pi}^{\pi} d\theta_2 \sum_k K_k e^{ik(\theta_2 - \theta_1)} \sum_{k'} \hat{p}_{k'} e^{ik'\theta} \left\{ \text{sgn} \left(\cos \left(\frac{\theta_2 - \theta_1}{2} \right) \right) \right\}^{k'} e^{-i\frac{k'}{2}(\theta_1 + \theta_2)}. \end{aligned} \quad (\text{A.11})$$

We convert the variables from (θ_1, θ_2) to $(\Theta = \frac{\theta_1 + \theta_2}{2}, \Psi = \frac{\theta_2 - \theta_1}{2})$ and the Jacobian is $d\theta_1 d\theta_2 = 2d\Theta d\Psi$. Then the above becomes

$$\begin{aligned} & 2 \sum_k \sum_{k'} K_k \hat{p}_{k'} e^{ik'\theta} \int_{-\pi}^{\pi} d\Psi e^{2ik\Psi} \left\{ \text{sgn}(\cos \Psi) \right\}^{k'} \int_{-\pi + |\Psi|}^{\pi - |\Psi|} d\Theta e^{-ik'\Theta} \\ &= 4 \sum_k K_k \hat{p}_0 \int_{-\pi}^{\pi} d\Psi e^{2ik\Psi} (\pi - |\Psi|) - 4 \sum_k \sum_{k' \neq 0} K_k \hat{p}_{k'} e^{ik'\theta} \int_{-\pi}^{\pi} d\Psi e^{2ik\Psi} \left\{ -\text{sgn}(\cos \Psi) \right\}^{k'} \frac{\sin(k'|\Psi|)}{k'}. \end{aligned} \quad (\text{A.12})$$

In the case of $k \neq 0$, the first integral on the right hand side of Eq. (A.12) is zero. Therefore, the first integral becomes

$$4 \sum_k K_k \hat{p}_0 \int_{-\pi}^{\pi} d\Psi e^{2ik\Psi} (\pi - |\Psi|) = 4K_0 \hat{p}_0 \int_{-\pi}^{\pi} d\Psi (\pi - |\Psi|) = 4\pi^2 K_0 \hat{p}_0 = 2\pi K_0, \quad (\text{A.13})$$

where $2\pi \hat{p}_0 = \int_{-\pi}^{\pi} d\theta \hat{p}(\theta) = 1$ because $\hat{p}(\theta)$ is the probability distribution. On the other hand, the second integral is

$$\begin{aligned} & -4 \sum_k \sum_{k' \neq 0} K_k \hat{p}_{k'} e^{ik'\theta} \int_{-\pi}^{\pi} d\Psi e^{2ik\Psi} \left\{ -\text{sgn}(\cos \Psi) \right\}^{k'} \frac{\sin(k'|\Psi|)}{k'} \\ &= -8 \sum_k \sum_{k' \neq 0} K_k \hat{p}_{k'} \frac{e^{ik'\theta}}{k'} \int_0^{\pi} d\Psi \cos(2k\Psi) \left\{ -\text{sgn}(\cos \Psi) \right\}^{k'} \sin(k'\Psi) \\ &= -8 \sum_k \sum_{k' \neq 0} K_k \hat{p}_{k'} \frac{e^{ik'\theta}}{k'} \int_0^{\pi} d\Psi \left\{ -\text{sgn}(\cos \Psi) \right\}^{k'} \frac{\sin((k' + 2k)\Psi) + \sin((k' - 2k)\Psi)}{2} \\ &= -4 \sum_k \sum_{k' \neq 0, \pm 2k} K_k \hat{p}_{k'} \frac{e^{ik'\theta}}{k'} \int_0^{\pi} d\Psi \left\{ -\text{sgn}(\cos \Psi) \right\}^{k'} \left\{ \sin((k' + 2k)\Psi) + \sin((k' - 2k)\Psi) \right\} \\ &= -4 \sum_k \sum_{k' \neq 0, \pm 2k} K_k \hat{p}_{k'} \frac{e^{ik'\theta}}{k'} ((-1)^{k'} - 1) \left(\frac{\cos(\frac{\pi}{2}(k' + 2k))}{k' + 2k} + \frac{\cos(\frac{\pi}{2}(k' - 2k))}{k' - 2k} \right) \\ &= 0, \end{aligned} \quad (\text{A.14})$$

because $\cos\left(\frac{\pi}{2}(k' \pm 2k)\right) = 0$ when $(-1)^{k'} - 1 \neq 0$ (k' is odd).

Thus, Eq. (A.9) reads

$$c\mathcal{I}\overline{f_0}^2 \left(1 - \frac{\delta\mathcal{I}(\mathbf{r}, t)}{\mathcal{I}}\right) \int_{-\pi}^{\pi} d\theta_1 \int_{-\pi}^{\pi} d\theta_2 K(\theta_2 - \theta_1) \hat{p}(\theta - \vartheta(\theta_1, \theta_2)) = 2\pi c\mathcal{I}\overline{f_0}^2 \left(1 - \frac{\delta\mathcal{I}(\mathbf{r}, t)}{\mathcal{I}}\right) K_0, \quad (\text{A.15})$$

which cancels out with Eq. (A.8). Therefore, the Boltzmann equation (Eq. (A.4)) becomes

$$\begin{aligned} \frac{\partial \delta f(\mathbf{r}, \theta, t)}{\partial t} = & -v_0 \mathbf{e}(\theta) \cdot \nabla \delta f(\mathbf{r}, \theta, t) \\ & -s \delta f(\mathbf{r}, \theta, t) + s \int_{-\pi}^{\pi} d\theta' p(\theta - \theta') \delta f(\mathbf{r}, \theta', t) \\ & -c\mathcal{I}\overline{f_0} \int_{-\pi}^{\pi} d\theta' K(\theta' - \theta) \\ & \times \left\{ \delta f(\mathbf{r}, \theta, t) + \frac{1}{\mathcal{I}} \int d^2\mathbf{r}' G_0(|\mathbf{r}' - \mathbf{r}|) B(|\mathbf{r}' - \mathbf{r}|) \delta f(\mathbf{r}', \theta', t) \right\} \\ & + c\mathcal{I}\overline{f_0} \int_{-\pi}^{\pi} d\theta_1 \int_{-\pi}^{\pi} d\theta_2 K(\theta_2 - \theta_1) \hat{p}(\theta - \vartheta(\theta_1, \theta_2)) \\ & \times \left\{ \delta f(\mathbf{r}, \theta_2, t) + \frac{1}{\mathcal{I}} \int d^2\mathbf{r}' G_0(|\mathbf{r}' - \mathbf{r}|) B(|\mathbf{r}' - \mathbf{r}|) \delta f(\mathbf{r}', \theta_2, t) \right\}. \end{aligned} \quad (\text{A.16})$$

3. Spatial integrals

Here we calculate the integral $\mathcal{I}\overline{f_0}$.

$$\mathcal{I}\overline{f_0} = \overline{f_0} \int d^2\mathbf{R} B(R) G_0(R) = \rho_0 \int_0^\infty dR R e^{-\frac{R^2}{2R_0^2}} \exp\left(-\rho_0 \int_0^R dR' \mathcal{D}(R')\right). \quad (\text{A.17})$$

By using Eq. (7), we get the integral in the exponential function:

$$\int_0^R dR' \mathcal{D}(R') = \begin{cases} \frac{R^2}{2} \Phi & [R < R_D], \\ R_D^2 \Phi \left(-\frac{3}{2} + 2\frac{R}{R_D} + \ln\left(\frac{R_D}{R}\right)\right) & [R > R_D], \end{cases} \quad (\text{A.18})$$

and then

$$\mathcal{I}\overline{f_0} = \rho_0 \int_0^{R_D} dR R e^{-\rho_0 \left(\Phi + \frac{1}{\rho_0 R_0^2}\right) \frac{R^2}{2}} + \rho_0 \int_{R_D}^\infty dR R e^{-\frac{R^2}{2R_0^2}} e^{-\rho_0 R_D^2 \Phi \left\{-\frac{3}{2} + 2\frac{R}{R_D} + \ln\left(\frac{R_D}{R}\right)\right\}}. \quad (\text{A.19})$$

The first integral is calculated as

$$\rho_0 \int_0^{R_D} dR R e^{-\rho_0 \left(\Phi + \frac{1}{\rho_0 R_0^2}\right) \frac{R^2}{2}} = \frac{1 - \exp\left(-\frac{\rho_0 R_D^2}{2} \left(\Phi + \frac{1}{\rho_0 R_0^2}\right)\right)}{\Phi + \frac{1}{\rho_0 R_0^2}}. \quad (\text{A.20})$$

This is zero for $\rho_0 = 0$, and approaches asymptotically $\frac{1}{\Phi} \left(1 - \frac{1}{\rho_0 \Phi R_0^2}\right)$ for $\rho_0 \rightarrow \infty$. On the other hand, the second integral is

$$\rho_0 \int_{R_D}^\infty dR R e^{-\frac{R^2}{2R_0^2}} e^{-\rho_0 \Phi R_D^2 \left\{-\frac{3}{2} + 2\frac{R}{R_D} + \ln\left(\frac{R_D}{R}\right)\right\}} = \rho_0 R_D^2 \int_1^\infty d\xi \xi e^{-\frac{R_D^2}{2R_0^2} \xi^2} \left(e^{\frac{3}{2}} \xi e^{-2\xi}\right)^{\rho_0 \Phi R_D^2}, \quad \xi = \frac{R}{R_D}. \quad (\text{A.21})$$

It is difficult to perform this integral analytically, but we can estimate its value. $e^{\frac{3}{2}} \xi e^{-2\xi}$ takes $e^{-\frac{1}{2}}$ as the maximum value at $\xi = 1$ in the interval of integral, and then

$$\rho_0 R_D^2 \int_1^\infty d\xi \xi e^{-\frac{R_D^2}{2R_0^2} \xi^2} \left(e^{\frac{3}{2}} \xi e^{-2\xi}\right)^{\rho_0 \Phi R_D^2} < \rho_0 R_D^2 e^{-\frac{1}{2} \rho_0 \Phi R_D^2} \int_1^\infty d\xi \xi e^{-\frac{R_D^2}{2R_0^2} \xi^2} = \rho_0 R_0^2 e^{-\frac{1}{2} \rho_0 \Phi R_D^2} e^{-\frac{R_D^2}{2R_0^2}}. \quad (\text{A.22})$$

This is zero for $\rho_0 = 0$, and converges to zero exponentially at $\rho_0 \rightarrow \infty$. Therefore, $\overline{\mathcal{I}f_0}$ takes a finite value. In the point particle limit $R_D = 0$ (in other words, the non occlusion case $G = 1$), we can calculate \mathcal{I} as the accurate form

$$\overline{\mathcal{I}f_0} = \rho_0 \int_0^\infty dR R e^{-\frac{R^2}{2R_0^2}} = \rho_0 R_0^2. \quad (\text{A.23})$$

Next, we calculate the integral

$$\frac{1}{\mathcal{I}} \int d^2 \mathbf{r}' G_0(|\mathbf{r}' - \mathbf{r}|) B(|\mathbf{r}' - \mathbf{r}|) e^{i\mathbf{q} \cdot \mathbf{r}'} = \frac{e^{i\mathbf{q} \cdot \mathbf{r}}}{\mathcal{I}} \int d^2 \mathbf{R} G_0(R) B(R) e^{i\mathbf{q} \cdot \mathbf{R}}, \quad (\text{A.24})$$

which is related with the spatial integral including δf in Eq. (A.16). This integration is also difficult to calculate analytically, but $G_0(R)$ and $B(R)$ is monotonically decreasing function of $R = \sqrt{R_x^2 + R_y^2}$, and thus

$$\hat{\mathcal{I}}(\mathbf{q}) := \frac{1}{\mathcal{I}} \int d^2 \mathbf{R} G_0(R) B(R) e^{i\mathbf{q} \cdot \mathbf{R}} = \frac{1}{\mathcal{I}} \int_{-\infty}^\infty dR_x \int_{-\infty}^\infty dR_y G_0(R) B(R) \cos(q_x R_x) \cos(q_y R_y) \quad (\text{A.25})$$

takes $-1 < \hat{\mathcal{I}}(\mathbf{q}) \leq 1$. When $\mathbf{q} = 0$, $\hat{\mathcal{I}}(\mathbf{q})$ takes the maximum value $\hat{\mathcal{I}}(0) = 1$, and when $\mathbf{q} \rightarrow \infty$, $\hat{\mathcal{I}}(\mathbf{q}) \rightarrow 0$. In the point particle limit $R_D = 0$,

$$\hat{\mathcal{I}}(\mathbf{q}) = e^{-\frac{q^2 R_0^2}{2}}. \quad (\text{A.26})$$

4. Fourier components of the Boltzmann equation

Except for the term including $\vartheta(\theta_1, \theta_2)$, the Fourier components (k, \mathbf{q}) of each term of Eq. (A.16) then become

$$\frac{\partial \delta f(\theta, t)}{\partial t} \rightarrow -\Lambda_k(\mathbf{q}) \delta f_k(\mathbf{q}, t) \quad (\text{A.27})$$

$$-v_0 \mathbf{e}(\theta) \cdot \nabla \delta f(\mathbf{r}, \theta, t) \rightarrow -\frac{v_0}{2} \{ (q_y + i q_x) \delta f_{k-1}(\mathbf{q}, t) - (q_y - i q_x) \delta f_{k+1}(\mathbf{q}, t) \} \quad (\text{A.28})$$

$$-s \delta f(\mathbf{r}, \theta, t) + s \int_{-\pi}^\pi d\theta' p(\theta - \theta') \delta f(\mathbf{r}, \theta', t) \rightarrow s(2\pi p_k - 1) \delta f_k(\mathbf{q}, t), \quad (\text{A.29})$$

$$\begin{aligned} & -c\overline{\mathcal{I}f_0} \int_{-\pi}^\pi d\theta' K(\theta' - \theta) \left(\delta f(\mathbf{r}, \theta, t) + \frac{1}{\mathcal{I}} \int d^2 \mathbf{r}' G_0(|\mathbf{r}' - \mathbf{r}|) B(|\mathbf{r}' - \mathbf{r}|) \delta f(\mathbf{r}', \theta', t) \right) \\ & \rightarrow -2\pi c\overline{\mathcal{I}f_0} \left(K_0 + \hat{\mathcal{I}}(\mathbf{q}) K_k \right) \delta f_k(\mathbf{q}, t). \end{aligned} \quad (\text{A.30})$$

The term including $\vartheta(\theta_1, \theta_2)$

$$c\overline{\mathcal{I}f_0} \int_{-\pi}^\pi d\theta_1 \int_{-\pi}^\pi d\theta_2 K(\theta_2 - \theta_1) \hat{p}(\theta - \vartheta(\theta_1, \theta_2)) \left(\delta f(\mathbf{r}, \theta_2, t) + \frac{1}{\mathcal{I}} \int d^2 \mathbf{r}' G_0(|\mathbf{r}' - \mathbf{r}|) B(|\mathbf{r}' - \mathbf{r}|) \delta f(\mathbf{r}', \theta_2, t) \right), \quad (\text{A.31})$$

is calculated as follows using the same techniques for Eq. (A.9). The Fourier components of \mathbf{q} are

$$\begin{aligned} & 2c\overline{\mathcal{I}f_0} \left(1 + \hat{\mathcal{I}}(\mathbf{q}) \right) \sum_k \sum_{k'} \sum_{k''} K_k \hat{p}_{k'} e^{ik'\theta} \delta f_{k''}(\mathbf{q}, t) \int_{-\pi}^\pi d\Psi e^{i(2k+k'')\Psi} \{ \text{sgn}(\cos \Psi) \}^{k'} \int_{-\pi+|\Psi|}^{\pi-|\Psi|} d\Theta e^{-i(k'-k'')\Theta} \\ & = 4c\overline{\mathcal{I}f_0} \left(1 + \hat{\mathcal{I}}(\mathbf{q}) \right) \sum_k \sum_{k'} K_k \hat{p}_{k'} e^{ik'\theta} \delta f_{k'}(\mathbf{q}, t) \int_{-\pi}^\pi d\Psi e^{i(2k+k')\Psi} \{ \text{sgn}(\cos \Psi) \}^{k'} (\pi - |\Psi|) \\ & \quad - 4c\overline{\mathcal{I}f_0} \left(1 + \hat{\mathcal{I}}(\mathbf{q}) \right) \sum_k \sum_{k'} \sum_{k'' \neq k'} K_k \hat{p}_{k'} e^{ik'\theta} \delta f_{k''}(\mathbf{q}, t) (-1)^{k''} \int_{-\pi}^\pi d\Psi e^{i(2k+k'')\Psi} \{ -\text{sgn}(\cos \Psi) \}^{k'} \frac{\sin((k' - k'')|\Psi|)}{k' - k''}, \end{aligned} \quad (\text{A.32})$$

where the second integral is zero for the same reason as Eq. (A.14). We consider only the first integral.

- In the case of $k' = -2k$, the first integral is

$$\begin{aligned} & 4c\mathcal{I}\overline{f_0} \left(1 + \hat{\mathcal{I}}(\mathbf{q})\right) \sum_k K_k \hat{p}_{-2k} e^{-2ik\theta} \delta f_{-2k}(\mathbf{q}, t) \int_{-\pi}^{\pi} d\Psi (\pi - |\Psi|) \\ &= 4\pi^2 c\mathcal{I}\overline{f_0} \left(1 + \hat{\mathcal{I}}(\mathbf{q})\right) \sum_k K_k \hat{p}_{-2k} e^{-2ik\theta} \delta f_{-2k}(\mathbf{q}, t). \end{aligned} \quad (\text{A.33})$$

- In the case of $k' \neq -2k$, the first integral is

$$\begin{aligned} & 4c\mathcal{I}\overline{f_0} \left(1 + \hat{\mathcal{I}}(\mathbf{q})\right) \sum_k \sum_{k' \neq -2k} K_k \hat{p}_{k'} e^{ik'\theta} \delta f_{k'}(\mathbf{q}, t) \int_{-\pi}^{\pi} d\Psi e^{i(2k+k')\Psi} \{\text{sgn}(\cos \Psi)\}^{k'} (\pi - |\Psi|) \\ &= 4c\mathcal{I}\overline{f_0} \left(1 + \hat{\mathcal{I}}(\mathbf{q})\right) \sum_k \sum_{k' \neq -2k} K_k \hat{p}_{k'} e^{ik'\theta} \delta f_{k'}(\mathbf{q}, t) \times 2(-1)^k \left\{ (1 - (-1)^{k'}) \left(\frac{\pi \sin(k'\frac{\pi}{2})}{2} \frac{1}{2k+k'} - \frac{\cos(k'\frac{\pi}{2})}{(2k+k')^2} \right) \right\} \\ &= 4c\mathcal{I}\overline{f_0} \left(1 + \hat{\mathcal{I}}(\mathbf{q})\right) \sum_k \sum_{k' \neq -2k} K_k \hat{p}_{k'} e^{ik'\theta} \delta f_{k'}(\mathbf{q}, t) \times 2\pi(-1)^k \frac{(-1)^{\frac{k'-1}{2}}}{2k+k'} \delta_{k', \text{odd}} \\ &= 8\pi c\mathcal{I}\overline{f_0} \left(1 + \hat{\mathcal{I}}(\mathbf{q})\right) \sum_k \sum_{k'} K_k \hat{p}_{k'} e^{ik'\theta} \delta f_{k'}(\mathbf{q}, t) \frac{(-1)^k (-1)^{\frac{k'-1}{2}}}{2k+k'} \delta_{k', \text{odd}}. \end{aligned} \quad (\text{A.34})$$

Thus, the Fourier components (k, \mathbf{q}) of Eq. (A.31) is

$$\rightarrow 2\pi c\mathcal{I}\overline{f_0} \left(1 + \hat{\mathcal{I}}(\mathbf{q})\right) \sum_{k'} K_{k'} (2\pi \hat{p}_{k'}) \delta f_{k'}(\mathbf{q}, t) \left(\delta_{k, -2k'} + \frac{2}{\pi} \frac{(-1)^{k'} (-1)^{\frac{k'-1}{2}}}{2k' + k} \delta_{k, \text{odd}} \right). \quad (\text{A.35})$$

5. Calculation of the damping rate

From Eqs. (A.27, A.28, A.29, A.30, A.35), we obtain the real part of the damping rate

$$\text{Re } \Lambda_k(\mathbf{q}) = s(1 - 2\pi p_k) + 2\pi c\mathcal{I}\overline{f_0} \left\{ (K_0 + \hat{\mathcal{I}}(\mathbf{q})K_k) - 2\pi \hat{p}_k \left(1 + \hat{\mathcal{I}}(\mathbf{q})\right) \sum_{k'} K_{k'} \left(\delta_{k, -2k'} + \frac{2}{\pi} \frac{(-1)^{k'} (-1)^{\frac{k'-1}{2}}}{2k' + k} \delta_{k, \text{odd}} \right) \right\}, \quad (\text{A.36})$$

where we set $v_0 = 0$ (without the advection term). When $\text{Re } \Lambda_k(\mathbf{q}) < 0$, the uniform distribution becomes unstable. Note that our aim is the derivation of the transition point, the cross term of $k \pm 1$ modes does not affect to the transition point itself. In fact, we confirm that this notion is successful, when we will see later the reproduction of the transition point of the local collision model as the singular case of our model (see Sect. V). Essentially, the advection term including the spatial derivative is not relevant to the transition point. (We provided the reason in the main text.)

Here, we assume that $p(\theta)$ (and $\hat{p}(\theta)$) are probability distributions that satisfies $0 < 2\pi p_k \leq 1$. For example, the von Mises distribution $p(\theta) = e^{\kappa \cos \theta} / (2\pi I_0(\kappa))$ takes $2\pi p_k = I_{|k|}(\kappa) / I_0(\kappa)$ where $I_{n=0,1,\dots}(\kappa)$ is the modified Bessel function of the first kind and the sharpness parameter $\kappa > 0$, and the wrapped Gaussian distribution $p(\theta) = \sum_{n=-\infty}^{\infty} \frac{1}{\sqrt{2\pi}\sigma} \exp\left(-\frac{(\theta+2\pi n)^2}{2\sigma^2}\right)$ takes $2\pi p_k = e^{-\sigma^2 k^2/2}$. When we adopt this probability distribution, the uniform distribution is stable when there is no interaction ($c = 0$).

In addition, we find that the uniform distribution is also stable when the orientational interaction does not depend on the relative angle ($K(\psi) = K_0 > 0$ and $K_{k \neq 0} = 0$). Therefore, $K(\psi)$ must have the deviation from a constant to arise the order. For $K(\psi) = \sqrt{2}|\sin \psi|$, K_k is

$$K_k = \frac{2\sqrt{2}}{\pi} \frac{\delta_{k, \text{even}}}{1 - k^2}, \quad (\text{A.37})$$

and then the related term is

$$\begin{aligned}
& 2\pi c \mathcal{I} \overline{f_0} \left\{ (K_0 + \hat{\mathcal{I}}(\mathbf{q}) K_k) - 2\pi \hat{p}_k \left(1 + \hat{\mathcal{I}}(\mathbf{q}) \right) \sum_{k'} K_{k'} \left(\delta_{k, -2k'} + \frac{2}{\pi} \frac{(-1)^{k'} (-1)^{\frac{k-1}{2}}}{2k' + k} \delta_{k, \text{odd}} \right) \right\} \\
&= 4\sqrt{2} c \mathcal{I} \overline{f_0} \left\{ \left(1 + \hat{\mathcal{I}}(\mathbf{q}) \frac{\delta_{k, \text{even}}}{1 - k^2} \right) - 2\pi \hat{p}_k \left(1 + \hat{\mathcal{I}}(\mathbf{q}) \right) \sum_{k'} \frac{\delta_{k', \text{even}}}{1 - k'^2} \left(\delta_{k, -2k'} + \frac{2}{\pi} \frac{(-1)^{k'} (-1)^{\frac{k-1}{2}}}{2k' + k} \delta_{k, \text{odd}} \right) \right\} \\
&= 4\sqrt{2} c \mathcal{I} \overline{f_0} \left\{ 1 + \hat{\mathcal{I}}(\mathbf{q}) \frac{\delta_{k, \text{even}}}{1 - k^2} - 2\pi \hat{p}_k \left(1 + \hat{\mathcal{I}}(\mathbf{q}) \right) \left(\frac{\delta_{\frac{k}{2}, \text{even}}}{1 - (\frac{k}{2})^2} + \frac{2\delta_{k, \text{odd}}}{4 - k^2} \right) \right\},
\end{aligned} \tag{A.38}$$

where

$$\begin{aligned}
& \sum_{k'=\text{even}} \frac{1}{(1 - k'^2)(2k' + k)} \\
&= \sum_{n=-\infty}^{\infty} \left(\frac{A_1}{4} \frac{1}{n + \frac{k}{4}} - \frac{A_2}{2} \frac{1}{n + \frac{1}{2}} - \frac{A_3}{2} \frac{1}{n - \frac{1}{2}} \right), \quad A_1 = \frac{4}{4 - k^2}, \quad A_2 = \frac{2 + k}{2(4 - k^2)}, \quad A_3 = \frac{2 - k}{2(4 - k^2)} \\
&= \pi \left(\frac{A_1}{4} \cot\left(\pi \frac{k}{4}\right) - \frac{A_2}{2} \cot\left(\frac{\pi}{2}\right) - \frac{A_3}{2} \cot\left(-\frac{\pi}{2}\right) \right) \\
&= \pi \frac{A_1}{4} \cot\left(\pi \frac{k}{4}\right) = \frac{\pi}{4 - k^2} (-1)^{\frac{k-1}{2}}.
\end{aligned} \tag{A.39}$$

Finally, we get

$$\text{Re } \Lambda_k(\mathbf{q}) = s(1 - 2\pi p_k) + 4\sqrt{2} c \mathcal{I} \overline{f_0} W_k(\mathbf{q}), \quad W_k(\mathbf{q}) := 1 + \hat{\mathcal{I}}(\mathbf{q}) \frac{\delta_{k, \text{even}}}{1 - k^2} - 2\pi \hat{p}_k \left(1 + \hat{\mathcal{I}}(\mathbf{q}) \right) \left(\frac{\delta_{\frac{k}{2}, \text{even}}}{1 - (\frac{k}{2})^2} + \frac{2\delta_{k, \text{odd}}}{4 - k^2} \right). \tag{A.40}$$

This equation does not depend on the sign of k . We remember $-1 < \hat{\mathcal{I}}(\mathbf{q}) \leq 1$ and $0 < 2\pi \hat{p}_k \leq 1$, and then

- In the case of $k = 1$, $W_1(\mathbf{q}) = 1 - \frac{2}{3} \times (2\pi \hat{p}_1) \left(1 + \hat{\mathcal{I}}(\mathbf{q}) \right)$.
- In the case of $k = \text{odd}$ and $k > 1$ ($k = 3, 5, 7, \dots$), $W_k(\mathbf{q}) = 1 + \frac{2}{k^2 - 4} (2\pi \hat{p}_1) \left(1 + \hat{\mathcal{I}}(\mathbf{q}) \right) > 0$.
- In the case of $k = \text{even}$ and $\frac{k}{2} \neq \text{even}$ ($k = 2, 6, 10, \dots$), $W_k(\mathbf{q}) = 1 - \frac{1}{k^2 - 1} \hat{\mathcal{I}}(\mathbf{q}) > 0$.
- In the case of $k = \text{even}$ and $\frac{k}{2} = \text{even}$ ($k = 4, 8, 12, \dots$), $W_k(\mathbf{q}) = 1 - \frac{1}{k^2 - 1} \hat{\mathcal{I}}(\mathbf{q}) + \frac{2}{(\frac{k}{2})^2 - 1} (2\pi \hat{p}_1) \left(1 + \hat{\mathcal{I}}(\mathbf{q}) \right) > 0$.

Therefore, $\text{Re } \Lambda_k(\mathbf{q})$ can be negative only if $k = 1$, and

$$\text{Re } \Lambda_1(\mathbf{q}) = s(1 - 2\pi p_1) - 4\sqrt{2} c \mathcal{I} \overline{f_0} \left\{ \frac{2}{3} \times (2\pi \hat{p}_1) \left(1 + \hat{\mathcal{I}}(\mathbf{q}) \right) - 1 \right\}. \tag{A.41}$$

$\hat{\mathcal{I}}(\mathbf{q}) = 1$ has a maximum at $\mathbf{q} = \mathbf{0}$, and then $\text{Re } \Lambda_1(\mathbf{q})$ can be negative in the case of $2\pi \hat{p}_1 > 3/4$, e.g. the sharpness parameter of the von Mises distribution is sufficiently large and the standard deviation parameter of the wrapped Gaussian distribution is sufficiently small. In this case, $\text{Re } \Lambda_1(\mathbf{q} = \mathbf{0})$ can be negative firstly as c increase.

We obtain the transition point by setting $\text{Re } \Lambda_1(\mathbf{q} = \mathbf{0}) = 0$, as

$$c_{\text{tr}} = \frac{s}{4\sqrt{2} \mathcal{I} \overline{f_0}} \frac{1 - 2\pi p_1}{\frac{4}{3} \times (2\pi \hat{p}_1) - 1} := \frac{c_0}{\mathcal{I} \overline{f_0}}. \tag{A.42}$$

Furthermore, due to $\hat{\mathcal{I}}(\mathbf{q}) < 1$ for $\mathbf{q} \neq \mathbf{0}$, $\text{Re } \Lambda_1(\mathbf{q} \neq \mathbf{0}) > 0$ at the transition point, and therefore the any spatial deviation from the uniform distribution attenuates at the transition point.

6. Limiting cases of the parameters

Here we consider the behavior of the transition point in the limit cases of parameters ρ_0 , R_D , R_0 .

First, when $\rho_0 \rightarrow 0$, $\mathcal{I}\overline{f}_0$ takes the asymptotic form $\mathcal{I}\overline{f}_0 \rightarrow \rho_0 R_0^2$ which is consistent with the point particle limit (Eq. (A.23)) due to reduced occlusion by dilution, and then c_{tr} becomes infinity as $c_{tr} \rightarrow c_0/(\rho_0 R_0^2)$. On the other hand, outside the application of the theory but we consider $\rho_0 \rightarrow \infty$ as a thought experiment, and $\mathcal{I}\overline{f}_0 \rightarrow 1/\Phi$, and thus c_{tr} has a non-zero value $c_{tr} \rightarrow c_0\Phi > 0$.

Next, we consider the point particle limit $R_D = 0$ ($G = 1$). In this case, $\mathcal{I}\overline{f}_0 = \rho_0 R_0^2$ (see Eq. (A.23)), and then we obtain the transition point $c_{tr} = c_0/(\rho_0 R_0^2)$. When $\rho_0 \rightarrow \infty$, $c_{tr} = 0$ for the non-occlusion case. Therefore, we can confirm that the effect of occlusion ($R_D \neq 0$) brings non-zero values of $c_{tr} \rightarrow c_0\Phi$. Moreover, for $R_D = 0$, we can directly calculate $\text{Re } \Lambda_1(\mathbf{q})$ at the transition point. From Eq. (A.41) and Eq. (A.42), we obtain

$$\begin{aligned} \text{Re } \Lambda_1(\mathbf{q}) &= s(1 - 2\pi p_1) - 4\sqrt{2}c_{tr}\mathcal{I}\overline{f}_0 \left\{ \frac{2}{3} \times (2\pi\hat{p}_1) \left(1 + e^{-\frac{q^2 R_0^2}{2}} \right) - 1 \right\} \\ &= 2s \frac{1 - 2\pi p_1}{4 \times (2\pi\hat{p}_1) - 3} \times (2\pi\hat{p}_1) \left(1 - e^{-\frac{q^2 R_0^2}{2}} \right) > 0. \end{aligned} \quad (\text{A.43})$$

Therefore, the any spatial deviation from the uniform distribution attenuates at the phase transition point due to the any slightly non-locality $R_0 > 0$.

Finally, in the case $R_0 \rightarrow \infty$ ($B = 1$), the integrals in $\mathcal{I}\overline{f}_0$ become

$$\rho_0 \int_0^{R_D} dR R e^{-\rho_0 \left(\Phi + \frac{1}{\rho_0 R_0^2} \right) \frac{R^2}{2}} \rightarrow \frac{1}{\Phi} \left(1 - e^{-\frac{\rho_0 \Phi R_D^2}{2}} \right), \quad (\text{A.44})$$

$$\begin{aligned} &\rho_0 \int_{R_D}^{\infty} dR R e^{-\frac{R^2}{2R_0^2}} e^{-\rho_0 \Phi R_D^2 \left\{ -\frac{3}{2} + 2\frac{R}{R_D} + \ln\left(\frac{R}{R_D}\right) \right\}} \\ &\rightarrow \rho_0 R_D^2 \int_1^{\infty} d\xi \xi \left(e^{\frac{3}{2}\xi} e^{-2\xi} \right)^{\rho_0 \Phi R_D^2}, \quad \xi = \frac{R}{R_D} \\ &= \rho_0 R_D^2 e^{\frac{3}{2}\rho_0 \Phi R_D^2} E_{-1-\rho_0 \Phi R_D^2}(2\rho_0 \Phi R_D^2), \end{aligned} \quad (\text{A.45})$$

where $E_a(z) = \int_1^{\infty} d\xi e^{-z\xi}/\xi^a$ is the generalized exponential integral and then we can obtain analytically

$$\mathcal{I}\overline{f}_0 \rightarrow \frac{1}{\Phi} \left(1 - e^{-\frac{\rho_0 \Phi R_D^2}{2}} \right) + \rho_0 R_D^2 e^{\frac{3}{2}\rho_0 \Phi R_D^2} E_{-1-\rho_0 \Phi R_D^2}(2\rho_0 \Phi R_D^2). \quad (\text{A.46})$$

Thus c_{tr} takes a non-zero value even though an agent can perceive a neighbor at infinite relative distance, due to the visual screening effect. In fact, at the point particle limit $R_D \rightarrow 0$, the generalized exponential integral has the asymptotic form $E_{-1-\rho_0 \Phi R_D^2}(2\rho_0 \Phi R_D^2) \rightarrow 1/(2\rho_0 \Phi R_D^2)^2$, and then $\mathcal{I}\overline{f}_0 \rightarrow \infty$ and $c_{tr} \rightarrow 0$.

-
- | | |
|---|---|
| <p>[1] T. Vicsek and A. Zafeiris, Phys. Rep. 517, 71 (2012).
 [2] V. H. Sridhar, L. Li, D. Gorbos, M. Nagy, B. R. Schell, T. Sorochnik, N. S. Gov, and I. D. Couzin, Proc. Natl. Acad. Sci. U.S.A. 118, e2102157118 (2021).
 [3] A. Strandburg-Peshkin, C. R. Twomey, N. W. F. Bode, A. B. Kao, Y. Katz, C. C. Ioannou, S. B. Rosenthal, C. J. Torney, H. S. Wu, S. A. Levin, and I. D. Couzin, Curr. Biol. 23, R709 (2013).
 [4] D. J. G. Pearce, A. M. Miller, G. Rowlands, and M. S. Turner, Proc. Natl. Acad. Sci. U.S.A. 111, 10423 (2014).
 [5] M. Moussaïd, D. Helbing, and G. Theraulaz, Proc. Natl. Acad. Sci. U.S.A. 108, 6884 (2011).
 [6] J. E. Herbert-Read, A. Perna, R. P. Mann, T. M. Schaerf,</p> | <p>D. J. T. Sumpter, and A. J. W. Ward, Proc. Natl. Acad. Sci. U.S.A. 108, 18726 (2011).
 [7] R. Dukas, Constraints on information processing and their effects on behavior, in <i>Cognitive Ecology: The Evolutionary Ecology of Information Processing and decision making</i> (University of Chicago Press, Chicago, 1998).
 [8] J. Jhawar, R. G. Morris, U. R. Amith-Kumar, M. D. Raj, T. Rogers, H. Rajendran, and V. Guttal, Nat. Phys. 16, 488 (2020).
 [9] T. Vicsek, A. Czirók, E. Ben-Jacob, I. Cohen, and O. Shochet, Phys. Rev. Lett. 75, 1226 (1995).
 [10] I.D. Couzin, J. Krause, R. James, G.D. Ruxton, and N.R. Franks, J. theor. Biol. 218, 1 (2002).</p> |
|---|---|

- [11] H. Chaté, F. Ginelli, G. Grégoire, and F. Raynaud, *Phys. Rev. E* **77**, 046113 (2008).
- [12] B. H. Lemasson, J. J. Anderson, and R. A. Goodwin, *J. Theor. Biol.* **261**, 501 (2009).
- [13] H. Kunz and C. K. Hemelrijk, *Appl. Anim. Behav. Sci.* **138**, 142 (2012).
- [14] R. Bastien and P. A. Romanczuk, *Sci. Adv.* **6**, eaay0792 (2020).
- [15] D. Castro, F. Ruffier, and C. Eloy, *Phys. Rev. Research* **6**, 023016 (2024).
- [16] B. Collignon, A. Séguret, and J. Halloy, *R. Soc. open sci.* **3**, 150473 (2016).
- [17] D. Gorbonos, N. S. Gov, and I. D. Couzin, *PRX Life* **2**, 013008 (2024).
- [18] S. Ito and N. Uchida, *PNAS Nexus* **3**, pgae264 (2024).
- [19] J. Toner and Y. Tu, *Phys. Rev. Lett.* **75**, 4326 (1995).
- [20] J. Toner and Y. Tu, *Phys. Rev. E* **58**, 4828 (1998).
- [21] E. Bertin, M. Droz, and G. Grégoire, *J. Phys. A: Math. Theor.* **42**, 445001 (2009).
- [22] A. Peshkov, S. Ngo, E. Bertin, H. Chaté, and F. Ginelli, *Phys. Rev. Lett.* **109**, 098101 (2012).
- [23] E. Bertin, A. Baskaran, H. Chaté, and M. C. Marchetti, *Phys. Rev. E* **92**, 042141 (2015).
- [24] A. Patelli, I. Djafer-Cherif, I. S. Aranson, E. Bertin, and H. Chaté, *Phys. Rev. Lett.* **123**, 258001 (2019).
- [25] F. Thüroff, C. A. Weber, and E. Frey, *Phys. Rev. X* **4**, 041030 (2014).
- [26] D. Pita, B. A. Moore, L. P. Tyrrell, and E. Fernández-Juricic, *PeerJ* **3**, e1113 (2015).
- [27] D. S. Calovi, A. Litchinko, V. Lecheval, U. Lopez, A. P. Escudero, H. Chaté, C. Sire, and G. Theraulaz, *PLOS Comput. Biol.* **14**, e1005933 (2018).
- [28] We adopt the von Mises distribution to $p(\theta)$, $\hat{p}(\theta)$, but our results do not change qualitatively in the case of the usual probability distribution satisfying $0 < p_k$, $\hat{p}_k \leq 1/(2\pi)$. See Appendix 5.
- [29] See Section I. of Supplementary Material for derivation of $\mathcal{D}(R)$.
- [30] See Fig. S2 for plots of the occlusion factor G for uniform density.
- [31] See Section III. of Supplemental Material, where we also confirmed that an alternative form of $K(\psi)$ does not qualitatively change the results.
- [32] R. Bainbridge, *J. Exp. Biol.* **35**, 109 (1958).
- [33] O. Akanyeti, J. Putney, Y. R. Yanagitsuru, G. V. Lauder, W. J. Stewart, and J. C. Liao, *Proc. Natl. Acad. Sci. U. S. A.* **114**, 13828 (2017).
- [34] See Section II of Supplemental Material for the details of parameter choice.
- [35] See Section IV of Supplemental Material for derivation of the scaling law, and Eq. (S22) for the expression of $P_0(c_{tr})$.
- [36] See Section V of Supplemental Material for the behavior of the model in the local limit $R_0 \rightarrow 0$.
- [37] D. Martin, H. Chaté, C. Nardini, A. Solon, J. Tailleur, and F. van Wijland, *Phys. Rev. Lett.* **126**, 148001 (2021); D. Martin, G. Spera, H. Chaté, C. Duclut, C. Nardini, J. Tailleur, and F. van Wijland, *J. Stat. Mech.* (2024) 084003.
- [38] P. Rahmani, F. Peruani, and P. Romanczuk, *Commun. Phys.* **4**, 206 (2021).
- [39] Ch. Becco, N. Vandewalle, J. Delcourt, P. Poncin, *Physica A* **367**, 487 (2006).
- [40] K. Tunström, Y. Katz, C. C. Ioannou, C. Huepe, and M. J. Lutz, I. D. Couzin, *PLoS Comput. Biol.* **9**, e1002915 (2013).
- [41] A. Costanzo and C. K. Hemelrijk, *J. Phys. D: Appl. Phys.* **51**, 134004 (2018).
- [42] J. Gautrais, C. Jost, M. Soria, A. Campo, S. Motsch, R. Fournier, S. Blanco, and G. Theraulaz, *J. Math. Biol.* **58**, 429 (2009).
- [43] S. Ito and N. Uchida, *J. Phys. Soc. Jpn.* **91**, 064806 (2022).
- [44] Y. Katz, K. Tunström, C. C. Ioannou, C. Huepe, and I. D. Couzin, *Proc. Natl. Acad. Sci. U.S.A.* **108**, 18720 (2011).